4-6-2018

Tuning the hydrophobic cores of self-immolative polyglyoxylate assemblies

Bo Fan
Western University

Rebecca E. Yardley
Western University

John F. Trant
Western University

Aneta Borecki
Western University

Elizabeth R. Gillies
Western University, egillie@uwo.ca

Polymer Chemistry

PAPER

Tuning the hydrophobic cores of self-immolative polyglyoxylate assemblies

Received 00th January 20xx,
Accepted 00th January 20xx

DOI: 10.1039/x0xx00000x

www.rsc.org/

Bo Fan,[a] Rebecca E. Yardley,[b] John F. Trant,[b] Aneta Borecki,[b] Elizabeth R. Gillies[ab*]

Polyglyoxylates are a recently-introduced class of self-immolative polymers, that depolymerize to small molecules upon the cleavage of a stimuli-responsive end-cap from the polymer terminus. The incorporation of different pendant ester groups or other aldehyde monomers offers the potential to tune the polymer properties, but this remains largely unexplored. With the goal of tuning the self-assembly and drug-loading properties of polyglyoxylate block copolymers, we explored the polymerization and copolymerization of *n*-butyl glyoxylate, L-menthyl glyoxylate, and chloral with ethyl glyoxylate to form UV light-responsive polyglyoxylates. The resulting polymers were coupled to poly(ethylene glycol) to afford amphiphilic block copolymers. Self-assembly of the different copolymers was studied and although each system formed solid particles, the cores of the assemblies differed in their stability, hydrophobicity, and their ability to load the hydrophobic drug celecoxib. All systems depolymerized and released the drug in response to UV light. The toxicity profiles for the assemblies were also evaluated using MDA-MB-231 cells. Overall, this work demonstrates that the properties of polyglyoxylates and their assemblies can be readily tuned through the incorporation of new monomers, thereby providing a promising platform for drug delivery and other applications.

Introduction

Biodegradable polymers such as poly(lactic acid), poly(caprolactone) and poly(glycolic acid) have been extensively studied over the past few decades as replacements for traditional non-degradable polymers.[1-3] In particular, these biodegradable polymers are of significant interest as biomedical materials such as sutures,[4] tissue engineering scaffolds,[2] and drug delivery vehicles.[5] Polyester nanoparticles have emerged as promising materials for the delivery of drugs, where they can address limitations of drugs such as poor water solubility, low stability, and toxic side effects.[6, 7] Thus far, several examples of polyester-based nanoparticles loaded with anti-cancer drugs have been approved for clinical trials in different countries, and Genexol™-PM, a formulation based on PEG-*b*-poly(D,L-lactic acid) with paclitaxel incorporated, has been approved by the FDA.[6, 8] However, the degradation of polyesters and the release of drugs from these systems are challenging to control and cannot be precisely controlled or "turned on" when needed.[9,10]

Stimuli-responsive polymers that can respond to external stimuli through degradation have been proposed as potential alternatives to polyesters.[11,12] Systems responsive to changes in pH[13,14] or temperature,[15] oxidation,[16] reduction,[17] light[18] and other stimuli have been explored and promising results have been achieved, particularly in drug delivery. Over the past decade, a new class of stimuli-responsive polymers, often referred to as "self-immolative polymers" (SIPs) has emerged.[19-21] SIPs are composed of a polymer backbone with stimuli-responsive end-caps at one or both termini. Cleavage of the end-cap results in reaction cascade leading to complete end-to-end depolymerization. One advantage of SIPs is their ability to amplify signals, as one stimulus event can generate hundreds of small molecules. This has led to proof-of-concept applications of SIPs in molecular sensors,[22] microcapsules,[23-25] point-of-care assay devices,[26] and drug delivery.[27,28] In addition, while traditional stimuli-responsive polymers require a substantial polymer redesign to change the stimulus to which the system responds, end-caps responsive to different stimuli can easily be introduced to SIPs while retaining the same backbone.[29] This makes each backbone relatively versatile. Backbones including polycarbamates,[22] polycarbonates,[30,31] poly(benzyl ether)s[32,33] and polyacetals[34,35] have been reported and end-caps responsive to stimuli including light,[27,34,36,37] redox agents,[27,29,38] enzymes,[22,39] and changes in pH[24,29] or temperature[40,41] have been incorporated.

In our previous work, we demonstrated that self-immolative poly(ethyl glyoxylate) (PEtG) could be coupled with hydrophilic poly(ethylene glycol) (PEG) via stimuli-responsive linker end-caps to form amphiphilic block copolymers.[28] These copolymers were self-assembled into nanoparticles that could load and release drugs in response to low concentrations of stimuli.

[a] *Department of Chemical and Biochemical Engineering and the Centre for Advanced Materials and Biomaterials Research, The University of Western Ontario, 1151 Richmond St., London, Ontario, Canada, N6A 5B9*
[b] *Department of Chemistry, The University of Western Ontario, 1151 Richmond St., London, Ontario, Canada, N6A 5B7*

Electronic Supplementary Information (ESI) available: [details of any supplementary information available should be included here]. See DOI: 10.1039/x0xx00000x

However, we found that the drug loading capabilities of PEtG-based particles were somewhat limited, ranging from 6.6 to 13 wt% depending on the drug. This limited drug loading was attributed to the relatively low hydrophobicity of PEtG. We hypothesized that it might be possible to tune the properties of the polyglyoxylate cores by incorporation of more hydrophobic glyoxylate monomers. Therefore, in this work we report the homopolymerization and copolymerization of *n*-butyl glyoxylate, L-menthyl glyoxylate, and chloral with ethyl glyoxylate to obtain new polyglyoxylates. These polyglyoxylates were incorporated into block copolymers and self-assembled to form particles. It is shown that these new assemblies have significantly improved drug loading capabilities, yet retain the important ability of SIPs to degrade and release drugs in response to external stimuli.

Experimental section

General materials

n-Butyl glyoxylate,[34] the linker end-cap,[34] PEG-N_3 (2 and 5 kg/mol),[42] and **PEtG-PEG2000**[28] (same batch used here) were synthesized as previously reported. Ethyl glyoxylate in toluene solution (50% w/w) and L-menthol were obtained from Alfa Aesar. Fumaryl chloride, dimethyl sulfide, chloral hydrate, and P_2O_5 were purchased from Sigma-Aldrich. Celecoxib was purchased from Ontario Chemicals Inc. Penstrep, fetal bovine serum (FBS), trypsin-EDTA (0.25%) and Dulbecco's modified Eagle medium (DMEM) with 4.5 g/L *D*-glucose and 110 mg/L sodium pyruvate were obtained from Gibco. NEt_3 and CH_2Cl_2 were distilled from CaH_2 before use. Anhydrous DMF was obtained from a solvent purification system using Al_2O_3 columns. Ethyl glyoxylate was purified as previously reported.[40] All the other chemicals were reagent grade and used without further purification unless otherwise noted.

General methods

^{1}H NMR spectra were obtained at 400 MHz or 600 MHz on Varian Inova instruments. NMR chemical shifts (δ) are reported in ppm and were calibrated against residual solvent signals of $CDCl_3$ (δ 7.27). Fourier transform infrared (FTIR) spectra were obtained in attenuated total reflectance mode using a PerkinElmer UATR Spectrum Two with films drop cast from CH_2Cl_2 on diamond. High-resolution mass spectrometry (HRMS) was performed with either a Thermo Scientific DFS (Double Focus Sector) mass spectrometer, using a reversed Nier Johnson geometry for electron impact (EI) ionization, or a Bruker microOTOF 11 for electrospray ionization (ESI). Size exclusion chromatography (SEC) was performed using a Viscotek GPC Max VE2001 solvent module equipped with a Viscotek VE3580 RI detector, two Agilent Polypore (300 × 7.5mm) columns connected in series and a Polypore guard column (50 × 7.5mm). Samples were dissolved in THF (glass distilled grade) at 5 mg/mL, filtered through 0.22 μm syringe filters, and injected using a 100 μL loop. The THF eluent was filtered and eluted at 1 mL/min. A calibration curve was obtained from poly(methyl methacrylate (PMMA) standards with molar masses of 1540-1,126,000 g/mol. Differential scanning calorimetry (DSC) was performed using a Q2000 from TA Instruments (New Castle, DE). The heating/cooling rate was 10 °C /min from -60 to +100 °C or -60 to +150 °C. Glass transition temperatures (T_g) were obtained from the second heating cycle. Thermogravimetric analyses (TGA) were performed on a TGA Q50 from TA Instruments. The heating rate was 10 °C/min between 30-500 °C under N_2. Dialyses were performed using Spectra/Por regenerated cellulose membranes with molecular weight cut-offs (MWCO) of either 2, 3.5, 6-8, 50 kg/mol. The hydrodynamic diameters of the polymer assemblies were measured by dynamic light scattering (DLS) using a Zetasizer Nano Series ZS instrument from Malvern Instruments with laser wavelength at 633 nm, at 25 °C in a 1 cm path length glass cuvette at a concentration of 1.0 mg/mL. TEM imaging was performed using a Phillips CM10 microscope operating at an acceleration voltage of 80 kV. 3 μL of micelle suspension (0.1 mg/mL) was placed onto a copper grid. The resulting sample was air-dried overnight before imaging. At least 40 particles were measured to obtain the mean particle diameters. Ultraviolet light irradiation was performed using an ACE Glass photochemistry cabinet containing a mercury light source (450 W bulb, 1.5 mW/cm^2 of UVA radiation and 0.06 mW/cm^2 of UVB radiation).

Synthesis of poly[(ethyl glyoxylate)-co-chloral] (PEtGC) and representative polymer synthesis procedure (additional procedures in the ESI)

First, chloral hydrate was converted to chloral. Chloral hydrate (10.0 g, 60 mmol, 1 equiv.) and P_2O_5 (8.5 g, 30 mmol, 0.5 equiv.) were mixed together under an N_2 atmosphere in a flamed-dried flask equipped with a magnetic stir bar. The flask was then heated in an oil bath, and the chloral hydrate started to melt when temperature reached 90 °C, resulting in its dehydration by P_2O_5. The resulting pale-yellow liquid (5.6 g, 64%) was collected using a short path distillation head when the temperature was ~ 110 °C at ambient pressure. The identity of the product was confirmed by ^{1}H NMR spectroscopy in $CDCl_3$ (δ = 9.05, s, 1H).[43] The purified chloral was then used for polymerization immediately. For the copolymer synthesis, purified ethyl glyoxylate (5.0 mL, 50.0 mmol, 1.0 equiv.) and chloral (1.0 mL, 9.5 mmol, 0.19 equiv.) were dissolved in CH_2Cl_2 (10.0 mL) and Et_3N (3.5 μL, 25 μmol, 0.0005 equiv.) was added. The solution was stirred for 1 h at -20 °C. Linker end-cap[34] (0.30 g, 1.0 mmol, 0.02 equiv.) suspended in CH_2Cl_2 (10.0 mL) and NEt_3 (0.2 mL, 1.5 mmol, 0.03 equiv.) was added at -20 °C to end-cap the polymer. The solution was gradually warmed to room temperature and then stirred for 16 h. The solution was then precipitated into methanol and the solvent was decanted. The resulting residue was dried in vacuo to provide a white sticky polymer (2.1 g, 35%). ^{1}H NMR (400 MHz, $CDCl_3$): δ 5.48-6.26 (m, 1.0 H), 4.15-4.31 (m, 1.9 H), 1.23-1.36 (m, 2.9 H). FTIR: 3058, 2986, 1756 cm^{-1}. SEC: M_n = 37 kg/mol, M_w = 55 kg/mol, $Đ$ = 1.5.

Synthesis of PEtGC-PEG2000 and representative procedure for the synthesis of an amphiphilic block copolymer

2 kg/mol PEG-N_3 (97 mg, 48.6 μmol, 6.0 equiv.) and **PEtGC** (300 mg, 8.1 μmol, 1.0 equiv.) were dissolved in DMF (5.0 mL) and then placed under an Ar atmosphere. $CuSO_4$ (4.0 mg, 28 μmol, 3.5 equiv.) and sodium ascorbate (5.0 mg, 28 μmol, 3.5 equiv.)

were then added and the mixture was stirred at 40 °C for 16 h. The reaction mixture was then transferred into a regenerated cellulose membrane (50 kg/mol MWCO) and dialyzed against deionized water for 16 h (1 L, 2 solvent changes) to remove DMF and most free PEG. The dialyzed material was then lyophilized, washed 3 times with water to further remove free PEG, and then dried to afford 300 mg (90% yield) of the product as a white rubbery solid. ^{1}H NMR (600 MHz, $CDCl_3$): δ 5.42-5.97 (m, 340 H), 4.10-4.30 (m, 697 H), 3.62 (s, 364 H), 3.36 (s, 5 H), 1.20-1.34 (m, 1054 H). FTIR: 3058, 2986, 2944, 2874, 1751, 1755 cm^{-1}. SEC: M_n = 41 kg/mol, M_w = 53 kg/mol, $Đ$ = 1.3.

Polymer self-assembly

10 mg of block copolymer was dissolved in 1.0 mL of DMSO with stirring overnight. 0.1 mL of the resulting solution was then rapidly injected into 0.9 mL of rapidly stirring deionized water. After stirring for 5 min, the suspension was dialyzed against deionized water for 24 h (2 x 1L) using a 3.5 kg/mol MWCO membrane to remove DMSO.

Measurement of the critical aggregation concentration (CAC)

A 1 mg/mL suspension of polymer assemblies was prepared as described above. 29 μL of a 0.1 mg/mL solution of Nile red in CH_2Cl_2 was added to each of a series of vials and then the solvent was evaporated to provide a thin film of Nile red. Next, 13 serial dilutions of the polymer suspension ranging from 1 to 2.5 x 10^{-4} mg/mL were added to the vials (1.5 mL/vial). The vials were then incubated at 37 °C overnight. Fluorescence emission spectra (520-700 nm) of each suspension were then measured using a QM-4 SE spectrometer from Photon Technology International (PTI) equipped with double excitation and emission monochromators. The excitation wavelength was 485 nm and the emission intensity at λ_{max} was record. The CAC was determined as the intercept of the two linear regions of the graph of fluorescence intensity vs. log(copolymer concentration).

Particle degradation studied by DLS.

Polymer assemblies were prepared as described above, except that the suspensions were dialyzed against 100 mM, pH 7.4 phosphate buffer for 24 h (2 x 1 L) instead of deionized water. The resulting polymer concentration was ~ 1.0 mg/mL. The count rate was measured by DLS while fixing the attenuator at 7. Then, the solution was divided in two. One half was kept in dark, while the other half was irradiated with UV light for 30 min. The samples were then incubated at 37 °C in the dark and the DLS count rate was measured at selected time points.

Loading of celecoxib.

10 mg of block copolymer and 3 mg of celecoxib were dissolved in 0.5 mL of DMF and stirred for 4 h. The solution was then rapidly injected into 9.5 mL of stirring deionized water and the resulting suspension was stirred for an additional 1 min at speed of 700 rpm. The suspension was then dialyzed against 100 mM, pH 7.4 phosphate buffer (2 x 1L) for 16 h using a 3.5 kg/mol MWCO membrane. It was then filtered through glass pipette containing a cotton filter to remove any unencapsulated and precipitated drug. 100 μL of the resulting particle suspension was diluted into 1.6 mL of acetonitrile to fully dissolve the copolymer and celecoxib, then the solution was filtered through a 0.20 μm syringe filter (Acrodisc Syringe Filter Non-Pyrogenic 13 mm, Pall Life Science) to remove any insoluble buffer salts. The absorbance at 250 nm was measured using a Varian UV/VIS Cary 300 spectrophotometer to calculate the celecoxib concentration (ε = 22884 L/mol·cm). This experiment was performed in triplicate and was used to calculate the loading efficiency and drug content, where:

Loading efficiency = (mass of loaded drug/mass of actual drug used) × 100%.

Drug content = (mass of loaded drug/mass of nanoparticles with drug) × 100%.

For analysis of the drug-loaded particles by TEM, the same procedure was used except that the particle suspension was dialyzed against deionized water instead of buffer.

Triggered release of celecoxib.

10 mL of drug-loaded polymer particle suspension (~1 mg/mL) was prepared as described above in pH 7.4 buffer, then was divided into two (5 mL) samples. One sample was irradiated for 30 min, and the other was kept in dark. They were then incubated in the dark at 37 °C. At selected time points, ~0.2 mL of the suspension was removed and filtered through a glass pipette containing a cotton filter to remove the released and precipitated celecoxib. 100 μL of the filtered suspension was then diluted into 1.6 mL of acetonitrile and the resulting suspension was filtered through a 0.20 μm syringe filter (Acrodisc Syringe Filter Non-Pyrogenic 13 mm, Pall Life Science) to remove any insoluble buffer salts. The absorbance of the acetonitrile solution at 250 nm was measured to determine the percentage of drug remaining in the assemblies. Each time point was measured in triplicate to calculate standard deviations.

In vitro cell toxicity assay.

Polymer particles were prepared for the assay at a concentration of 10 mg/mL in deionized water using the procedure as described above, except at 10-fold higher polymer concentration. The suspension was then either irradiated with UV light for 30 min or not irradiated. It was diluted 10-fold with DMEM containing 10% FBS and 100 units/mL of Penstrep to 1 mg/mL and then serial 2-fold dilutions were performed using the same medium. MDA-MB-231 cells were cultured in DMEM with 10% FBS and 100 units/mL of Penstrep in an atmosphere of 5% CO_2 at 37 °C. The cells were seeded in a 96 well plate (Corning Flat Bottom Plate) at a density of 5,000 cells/well and allowed to adhere for 24 h. The medium was then aspirated and replaced with various concentrations of particles, 0.2-0.05 mg/mL sodium dodecyl sulfate (positive control) or medium (negative control). The cells were incubated at 37 °C for 48 h. The medium was then aspirated and replaced with 100 μL of fresh medium containing 0.5 mg/mL (3-(4,5-dimethylthiazol-2-yl)-2,5-diphenyltetrazolium bromide) (MTT) reagent and the cells were incubated. After 4 h the plate was removed and the MTT reagent solution was aspirated. 50 μL of DMSO was added to each well to solubilize the formazan metabolic product of MTT. The plate was then placed in a plate reader (Tecan Infinite M1000 Pro) and the absorbance at 540 nm was measured to quantify the relative metabolic activities of the cells.

Results and discussion

Polymer synthesis

In addition to ethyl glyoxylate (**EtG**), three other aldehyde monomers were studied (Fig. 1). *n*-Butyl glyoxylate (**BuG**) is an analogue of ethyl glyoxylate, but with a longer aliphatic chain, making it more hydrophobic. L-Menthyl glyoxylate (**MenG**) is another hydrophobic analogue but is derived from a chiral and bioactive alcohol, making it of interest.[44] Chloral (**C**) is not a glyoxylate, but has three chloro groups α to the aldehyde, making it susceptible to polymerization while at the same time being hydrophobic.[45] **EtG** was purchased and purified as previously reported.[40] **C** was purchased as its hydrate and then distilled over P_2O_5 to afford the aldehyde. **BuG** was synthesized as previously reported.[34] **MenG** was synthesized via ozonolysis of its corresponding fumarate derivative (Scheme S1).

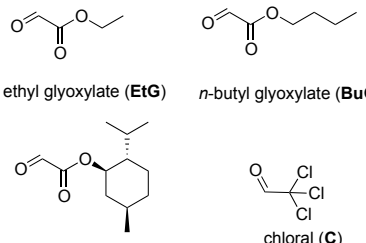

Fig. 1. Chemical structures of the monomers used in the current work.

Table 1. SEC and thermal analysis results for the polymers. [a]From SEC; [b]From TGA; [c]From DSC; [d]From previously published work.

Polymers	M_n (kg/mol)[a]	$Đ$[a]	T_o (°C)[b]	T_g (°C)[c]
PEtG[d]	42	2.1	200	-5
PEtBuG	30	2.1	226	-11
PMenG	2.0	1.3	235	58
PEtMenG	34	1.4	230	24 (T_m = 60)
PEtGC	37	1.5	133	3

Next, the polymerization of the monomers was investigated. The polymerization reactions were conducted at -20 °C with trace NEt_3 and EtG hydrate as an initiator (Scheme 1, Table 1). After polymerization, the polymers were end-capped *in situ* with a UV light-responsive *o*-nitrobenzyl chloroformate derivative having an alkyne functional handle for subsequent conjugation of the PEG block.[34] The resulting polymers were isolated by precipitation in methanol or dialysis against 1:1 acetone:methanol. Poly(ethyl glyoxylate) (**PEtG**) was synthesized as previously reported.[28] We have previously reported that homopolymerization of **BuG** gave low molar mass polymers, but that copolymerization with **EtG** afforded high molar masses with good incorporation of **BuG**.[34] Here we copolymerized **EtG** and **BuG** in a 1.5:1 molar ratio (Scheme 1a). Based on ^{1}H NMR spectroscopy, the resulting copolymer **PEtBuG** had a 1.9:1 mole ratio of the monomers, in reasonable agreement with the feed ratio. The number average molar mass (M_n) was 30 kg/mol and the dispersity ($Đ$) was 2.1 as measured by SEC in THF relative to PMMA standards. **MenG** was homopolymerized to afford **PMenG** with an M_n of 2.0 kg/mol and a $Đ$ of 1.3 (Scheme 1b), but copolymerization of a 2:1 ratio of **EtG**:**MenG** provided the copolymer **PEtMenG** with an M_n of 34 kg/mol, $Đ$ of 1.4 and a 1.6:1 ratio of **EtG**:**MenG** (Scheme 1c). It is known that the homopolymerization of chloral leads to predominately an isotactic 4/1-helical structure in the crystalline state, and it is insoluble in all solvents.[46] Therefore, we initially attempted the polymerization of a 1:1 ratio of **EtG**:**C**. The resulting copolymer precipitated from solution and could not be re-dissolved for analysis. Subsequently, we reduced the molar ratio to 3:1 **EtG**:**C**, but the resulting copolymer still had poor solubility in organic solvents such as CH_2Cl_2 and DMSO. Therefore, we polymerized a 5:1 ratio of **EtG**:**C** (Scheme 1d). The resulting copolymer **PEtGC** had an M_n of 37 kg/mol, $Đ$ of 1.5, and a 19:1 ratio of **EtG**:**C**. The chloral content was much lower than that expected based on the monomer feed ratios, suggesting that the aldehyde of the **C** monomer was much less susceptible to polymerization than that of **EtG**, perhaps due to sterics associated with the three chlorine groups on the adjacent carbon.

The thermal properties of the polymers were studied by TGA and DSC (Table 1, Figures S17-S22). Complete end-capping of the isolated polymers was confirmed by the fact that all of the polymers had onset degradation temperatures (T_o) higher than 100 °C. We have previously observed that non-capped polyglyoxylates began depolymerizing below 100 °C.[34] The T_o values for **PEtG**, **PEtBuG**, **PEtMenG**, and **PMenG** ranged from 200 to 235 °C while **PEtGC** had a T_o of 133 °C. This suggests that the chloral component of the polymer substantially reduced the thermal stability. As all of the polymers had the same end-cap, this suggests that introduction of the trichloromethyl moiety introduces a thermally labile bond along the backbone that can initiate degradation upon cleavage. **PEtG** had a T_g of -5 °C, while **PEtBuG** had a T_g of -11 °C due to the introduction of flexible side chains. **PMenG** had a T_g of 57 °C, while **PEtMenG** had a T_g of 24 °C. The increase in T_g for the menthyl-functionalized polymers can be attributed to the rigid cyclic structure of the menthyl moiety. **PEtMenG** also had a T_m of 60 °C. L-Menthol is a crystalline solid with a melting point of 41-44 °C, so crystallinity of the polymer likely arose from the menthyl moieties. It is possible that **PMenG** also had a T_m that was out of the range of the analysis (-60 – 150 °C, limited by the thermal stability of the polymers). **PEtGC** had a T_g of 3 °C, indicating that incorporation of the chloral moiety decreased segmental motion in the polymer, even at low monomer ratios.

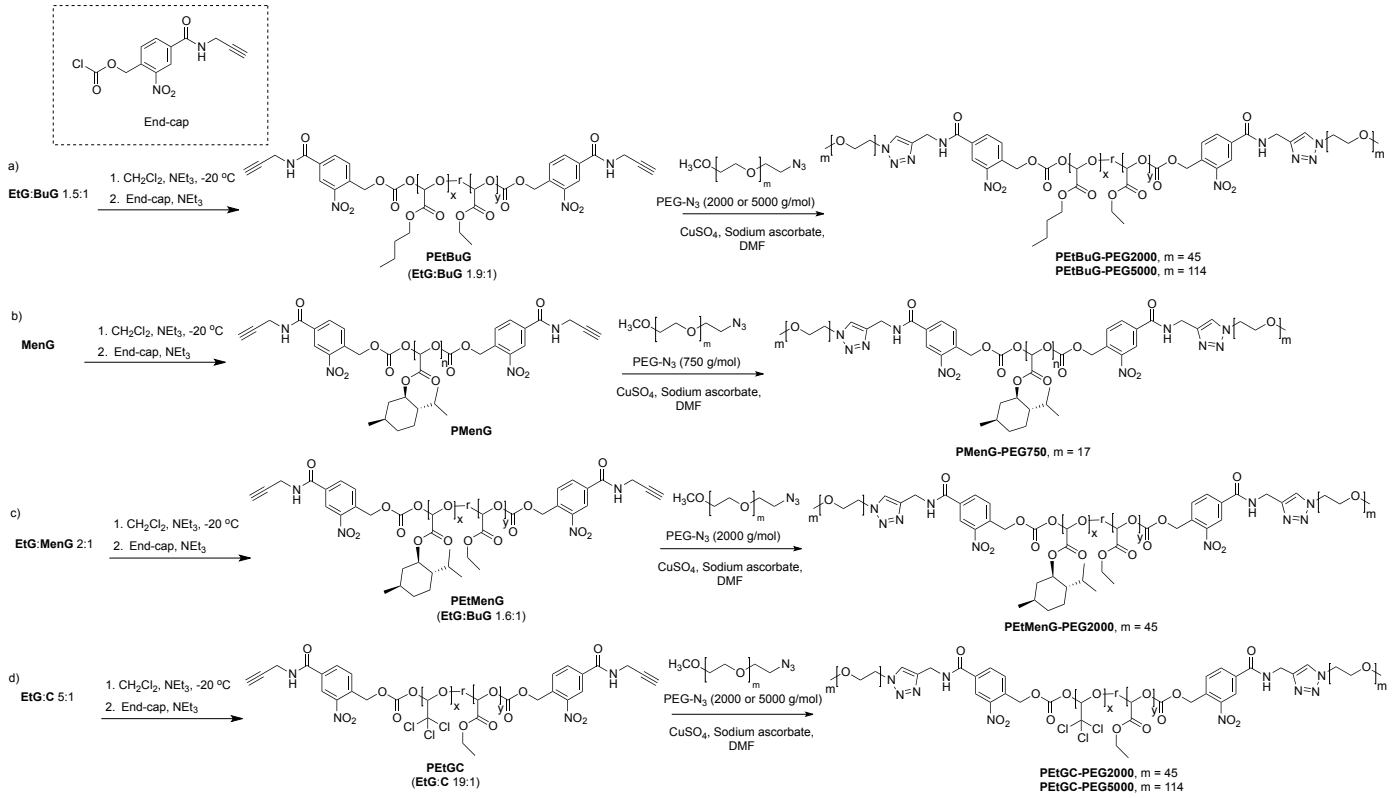

Scheme 1. Synthesis of polymers a) **PEtBuG**; b) **PMenG**; c) **PEtMenG**; d) **PEtGC** and corresponding block copolymers via coupling of PEG-N_3.

Next, the polymers were converted to amphiphilic block copolymers by the conjugation of PEG to the alkyne moieties on the end-caps. PEG has been widely used as hydrophilic polymer for biomedical applications due to its high biocompatibility in various applications.[47] The coupling reactions were conducted via copper-assisted akyne-azide cycloaddition reactions in DMF using azide-terminated PEG (PEG-N_3) (Scheme 1). It should be noted that because the polymerization was initiated with the glyoxylate hydrate, there were end-caps on both termini and consequently the coupling resulted in the formation of triblock copolymers (PEG-polyglyoxylate-PEG). In order to study the influence of different hydrophilic mass fractions (*f*), **PEtBuG** and **PEtGC** were each coupled with 2 and 5 kg/mol PEGs to afford **PEtBuG-PEG2000**, **PEtBuG-PEG5000**, **PEtGC-PEG2000** and **PEtGC-PEG5000** (Table 2). **PEtMenG** was coupled with 2 kg/mol PEG to afford **PEtMenG-PEG2000**. Because of its short hydrophobic block length, **PMenG** was coupled with 750 g/mol PEG to afford **PMenG-PEG750**. In all cases, the excess of PEGs were removed by dialysis and water washes. The purified block copolymers were characterized by ^{1}H NMR spectroscopy and SEC. Removal of uncoupled PEG was confirmed by SEC as no peaks corresponding to free PEG were observed (Figure S23-S28) and the expected fractions of PEG were observed in NMR spectroscopy (Figure S11-S16). The *f* values ranged from 0.11 – 0.39.

Block copolymer self-assembly

Self-assembly was performed via nanoprecipitation. Specifically, 0.1 mL of 10 mg/mL polymer solution in DMSO was injected into 0.9 mL of rapidly stirring water. After stirring for 5 min, the assemblies were dialyzed against water to remove DMSO. The critical aggregation concentrations (CACs) of these assemblies were determined by encapsulation of Nile red. The CACs were all similar, ranging from 40 to 79 mg/L. However, as expected the assemblies with higher *f* values also had higher CACs (Table 2). In addition, for very similar *f* values of 0.10-0.11, the CACs were lower for the more hydrophobic polymers such as **PEtBuG-PEG2000**, **PEtMenG-PEG2000**, and **PEtGC-PEG2000** than for the previously reported **PEtG-PEG2000**. The maximum emission wavelength (λ_{max}) of encapsulated Nile red can also serve as an indicator of the polarity of the environment at the core of the assembly, with a shift to shorter λ_{max} indicative of a more less polar environment. At an assembly concentration of 1 mg/mL, λ_{max} ranged from 586 – 600 nm, with the assemblies having a lower CAC values, such as **PEtMenG-PEG2000**, **PEtGC-PEG2000**, and **PEtBuG-PEG2000**, also having lower λ_{max}. Overall, these results suggest that it was possible to tune the hydrophobicity of the assembly cores.

Table 2. Characterization data for the amphiphilic block copolymers and their resulting assemblies. [a]Previously reported; [b]From SEC; [c]Measured at 1 mg/mL of copolymer.

Block copolymer	M_n[b] (kg/mol)	$Đ$[b]	f	CAC (mg/L)	Nile red λ_{max} (nm)[c]	Mean diameter from TEM (nm)	Z-average diameter from DLS (nm)
PEtG-PEG2000[a]	40	2.1	0.10	79	598	53 ± 17	82 ± 2
PEtBuG-PEG2000	36	1.9	0.11	47	595	37 ± 11	105 ± 23
PEtBuG-PEG5000	42	1.9	0.24	64	597	91 ± 107	110 ± 14
PMenG-PEG750	5.9	1.2	0.39	64	600	39 ± 7	173 ± 17
PEtMenG-PEG2000	35	1.5	0.11	52	586	38 ± 12	127 ± 26
PEtGC-PEG2000	41	1.4	0.10	40	591	31 ± 16	139 ± 142
PEtGC-PEG5000	36	1.3	0.28	62	594	157 ± 95	118 ± 21

The assemblies were also characterized by dynamic light scattering (DLS) and transmission electron microscopy (TEM) (Figure 2, Figures S36-S42). Based on DLS, the hydrodynamic diameters ranged from 82 - 173 nm, with polydispersity indices (PDIs) of 0.12 - 0.37 (Table 2). Based on TEM (Figure 2 and Figure S42), all of these assemblies were solid-core particles with average diameters ranging from 37 – 157 nm. The diameters measured by TEM were generally smaller than those measured by DLS, which can result from differences between the hydrated and dried states, and possible aggregation of assemblies in the suspensions used for DLS measurements. While longer PEG chains and higher f values would be expected to more effectively stabilize the assemblies, TEM images showed that the particles with longer PEG blocks aggregated to form larger particles. This was reproducible across multiple experiments, and might be attributed to interactions of particle coronas during drying. As their appeared to be no significant advantages of having the longer PEG block based on TEM or DLS, further studies focused on the 2 kg/mol PEG copolymers.

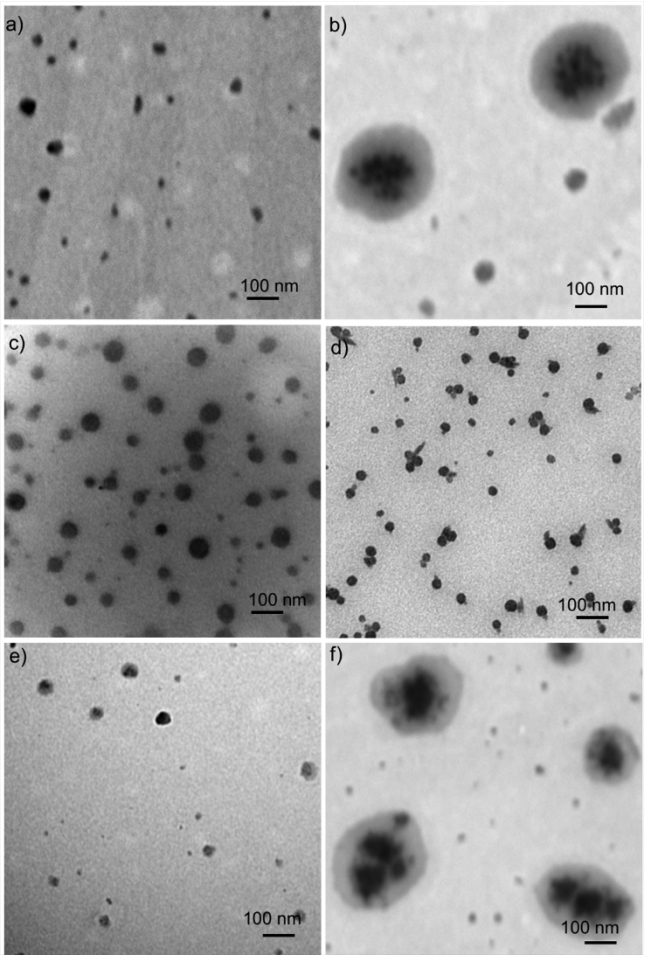

Fig. 2. TEM images of particles formed from (a) PEtBuG-PEG2000, (b) PEtBuG-PEG5000, (c) PEtMenG-PEG2000, (d) PMenG-PEG750. (e) PEtGC-PEG2000, (f) PEtGC-PEG5000.

Particle depolymerization

Due to the presence of the UV light-responsive linker end-cap in each block copolymer, the hydrophobic blocks were expected to depolymerize upon irradiation with UV light, resulting in disassembly of the particles. In order to verify this, the particles were suspended in pH 7.4 phosphate buffer at a concentration of 1 mg/mL, then irradiated with 1.5 mW/cm^2 of UVA light for

30 min. Controls consisted of non-irradiated particles. Particle disassembly was monitored based on the DLS count rate, which is proportional to particle number and particle mass when the attenuator is fixed at constant value. Thus, depolymerization would be expected to result in a decrease in the count rate. As shown in Fig. 3, without UV irradiation all of the particles were relatively stable in pH 7.4 at 37 °C for 24 h, with less than 20% reduction in count rate. However, after irradiation the particles disassembled almost immediately, leading to more than a 70% reduction in count rate over the first 2 h. Thus, the particles were indeed responsive to the light stimulus.

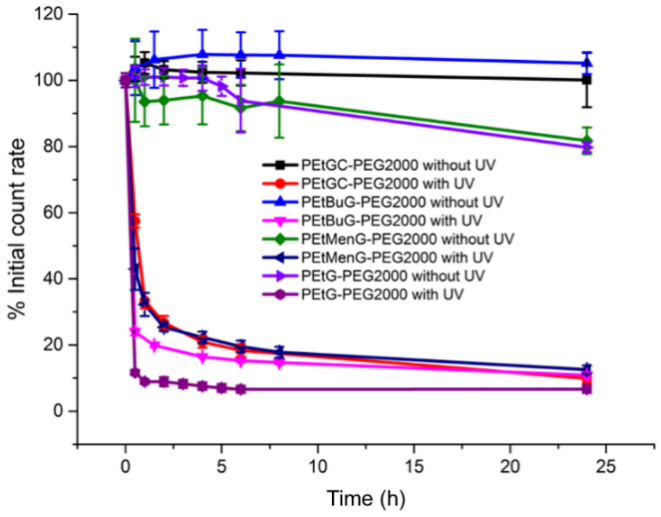

Fig. 3. Depolymerization of particles following UV light irradiation (or no light for controls), monitored by DLS based on count rate.

Celecoxib loading and release

Celecoxib is anti-inflammatory drug that is used in the treatment of arthritis, and has also shown potential as a chemotherapeutic.[48] However, it is limited by adverse side effects and low solubility (less than 3.3 mg/L), suggesting it could benefit from a drug delivery system. Therefore, celecoxib was loaded into the polymer assemblies. Drug loading was performed during the self-assembly process, with celecoxib co-dissolved in the organic phase with the polymer prior to nanoprecipitation. In contrast to the assemblies without drug where DMSO performed best as the organic solvent, DMF was found to be the best solvent for preparing celecoxib-loaded assemblies with diameters less than 100 nm and high drug loading.

As shown in Table 3, there were significant differences between the celecoxib content and loading efficiency for the different block copolymer assemblies. **PEtBuG-PEG2000** and **PEtMenG-PEG2000** assemblies had the highest celecoxib content at ~15 wt%, corresponding to a loading efficiency of ~60%. This suggests that the incorporation of hydrophobic comonomers improved the loading of hydrophobic drugs, likely because the assembly cores became more hydrophobic. **PEtGC-PEG2000** assemblies had the lowest celecoxib loading of only 6 wt%, corresponding to a loading efficiency of 21%. Although the cores of these assemblies were relatively hydrophobic based on the CAC values and the Nile red λ_{max}, the chloride groups on the chloral monomer may not have good compatibility with celecoxib. **PEtG-PEG2000** assemblies had an intermediate drug content of 10 wt% and a loading efficiency of 37%, which was significantly higher than **PEtGC-PEG2000** and significantly lower than **PEtBuG-PEG2000** and **PEtMenG-PEG2000**. To confirm that the *f* value didn't have a significant influence on the drug content, celecoxib was also loaded into **PEtBuG-PEG5000** assemblies. The resulting celecoxib content was ~14 wt%, and not significantly different from that of **PEtBuG-PEG2000**. Thus, the chemical structure of the core block, rather than the block ratios dominates the loading efficiency.

Table 3. Size characterization and celecoxib loading data for the block copolymer assemblies containing drug.

Block copolymers	Mean diameter from TEM (nm)	Z-average diameter from DLS (nm)	PDI (from DLS)	Drug loading content (%)	Drug loading efficiency (%)
PEtG-PEG2000	19 ± 8	63 ± 1	0.16 ± 0.01	10.0 ± 2.6	37.4 ± 10.8
PEtBuG-PEG2000	20 ± 10	51 ± 1	0.14 ± 0.01	15.0 ± 3.2	59.0 ± 15.1
PEtMenG-PEG2000	39 ± 12	52 ± 9	0.15 ± 0.09	15.1 ± 5.2	60.0 ± 23.3
PEtGC-PEG2000	34 ± 31	97 ± 2	0.16 ± 0.01	5.9 ± 3.9	21.2 ± 15.1

The drug-loaded assemblies were also characterized by TEM and DLS. TEM indicated that the **PEtG-PEG-2000**, **PEtBuG-PEG2000**, and **PEtMenG-PEG2000** assemblies remained as spherical particles after drug encapsulation (Figure S47). **PEtGC-PEG2000** assemblies were somewhere irregularly shaped, suggesting that the morphology was altered by celecoxib incorporation (Figure S47d). This may be related to the poor compatibility between celecoxib and the hydrophobic block, which was also reflected in the low drug loading content. The Z-average diameters measured by DLS were all lower than those for the non-loaded assemblies and ranged from 51 – 97 nm.

Next, the stimulus-mediated release of celecoxib from the particles was studied. Drug-loaded assemblies suspended in pH 7.4 phosphate buffer were either stored in the dark to serve as controls or were irradiated for 30 min. Upon release from the assemblies, celecoxib precipitated due to its low aqueous solubility. At each time point, the precipitated drug was removed by filtration and the percentage of drug remaining suspended in the assemblies was measured.

All of these particles released celecoxib much more rapidly following irradiation with UV light than without irradiation (Fig. 4). **PEtG-PEG2000** and **PEtMenG-PEG2000** released more than 70% of the celecoxib over the first 3 h. **PEtBuG-PEG2000** and **PEtGC-PEG2000** had more gradual release profiles, with ~40% and 50% respectively of the drug released over 3 h. The DLS

results had indicated that all the particles disassembled very rapidly after irradiation. Therefore, the different apparent rates of drug release may be related to the drug crystallization process. For the cases where rapid celecoxib release was measured, it was observed that large celecoxib crystals were formed. This precipitate sedimented, resulting in a clear solution containing the PEG block and water-soluble small molecule depolymerization products. For the cases with apparent slow release of drug, the solution turbidity increased dramatically after irradiation, suggesting the formation of small celecoxib crystals that did not sediment. Based on the filtration process employed in our release assay, the larger drug crystals would have been filtered off more efficiently, whereas the smaller crystals would have remained, appearing as non-released drug until they formed larger aggregates. It is known that the presence of small molecules in solution can influence the size of celecoxib crystals,[49,50] so differences in depolymerization products may have influenced the crystallization and consequently the precipitation of the drug. To probe this further, we obtained IR spectra of mixtures of the polymer and celecoxib. In the case of **PEtGC-PEG2000**, we observed a shift in the C=O stretch of the aldehyde monomer in the presence of the drug, which is consistent with a drug-monomer interaction (Fig. S49). However, for the other polymers, the ester C=O stretch dominated this region, so interactions could not be detected (Fig. S48, S50-S51). In any case, after 24 h, all of the triggered systems had released ~80% of the celecoxib.

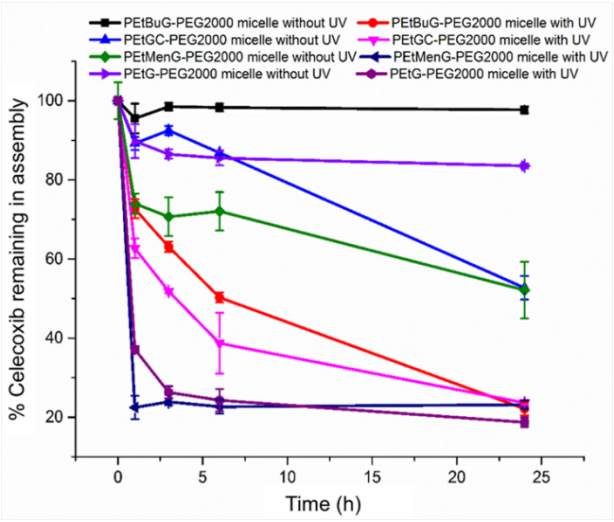

Fig. 4. Release of celecoxib over time for assemblies irradiated with UV light and for the corresponding systems stored in the dark.

Non-triggered systems that were stored in the dark released celecoxib more slowly. **PEtBuG-PEG2000** most effectively retained the drug, with less than 5% released over 24 h. This suggests that the flexible hydrophobic butyl chains likely were not only favorable for obtaining high drug loadings, but also for retaining the drug in the absence of stimulus. Non-triggered **PEtG-PEG2000** assemblies released ~20% of their celecoxib over 24 h, while **PEtMenG-PEG2000** and **PEtGC-PEG2000** released ~45%. These rates were much slower than the analogous irradiated systems, but suggest that the chemical structure of the core-forming block has a significant influence on the retention of drug.

In vitro toxicity studies

The toxicity of each of the non-loaded assemblies was investigated using MDA-MB-231 human breast cancer cells. Each system was evaluated in its irradiated and non-irradiated form following a 48 h incubation with the cells. In the absence of irradiation, **PEtMenG-PEG2000** and **PMenG-PEG750** assemblies showed minimal toxicity, with a high cell metabolic activity of >80% relative to control cells even at a concentration 1 mg/mL (Fig. 5). Non-triggered **PEtG-PEG2000**, **PEtBuG-PEG2000**, **PEtBuG-PEG5000** assemblies had similar effects on cells, with 60% metabolic activity at a concentration of 1 mg/mL. **PEtGC-PEG2000** and **PEtGC-PEG5000** assemblies showed higher toxicity with only ~30% metabolic activity remaining at 1 mg/mL.

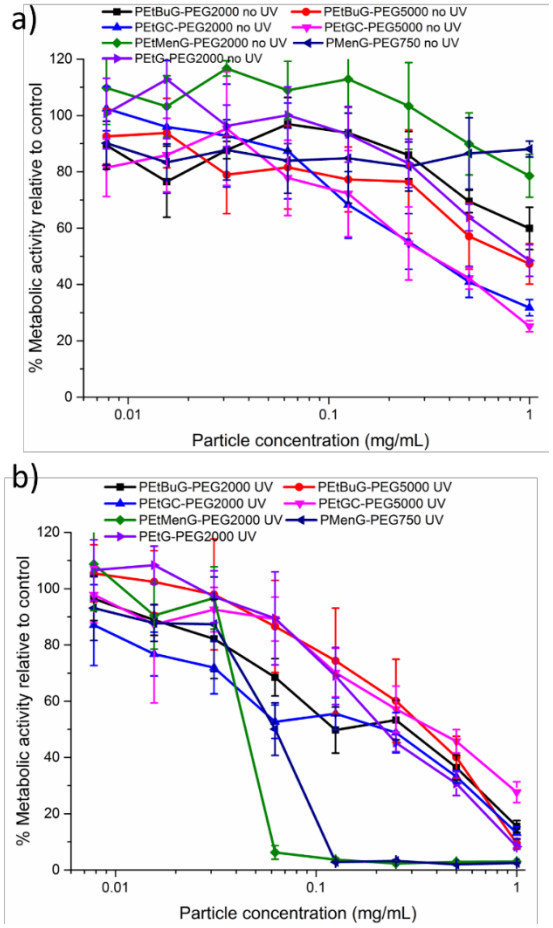

Fig. 5. Metabolic activities, measured by MTT assays of a) particles before UV irradiation and b) after UV irradiation.

After irradiation, all the assemblies exhibited higher toxicities compared to the non-triggered particles. Irradiation-induced depolymerization would produce the corresponding

glyoxylate and chloral monomers, which would be rapidly hydrated and hydrolyzed to glyoxylate or chloral hydrate and ethanol, *n*-butanol or L-menthol. Glyoxylate and ethanol can be metabolized in the liver but not in this cancer cell line.[51,52] This may explain why some toxicity was observed in this assay (IC_{50} ~250 μg/mL), but not in whole organism studies previously reported.[53] Like ethanol, *n*-butanol occurs in a number of alcoholic beverages and is considered have relatively low toxicity.[54] It is also metabolized by alcohol dehydrogenase in the liver. Chloral hydrate is used as a sedative for dental or medical treatments and has been administered to humans in gram-scale doses.[55] However, it is metabolized to trichloroethanol and trichloroethanol glucuronide in red blood cells and in plasma,[56] which would likely not happen in the current cell line and may explain why some toxicity to cells was observed. Interestingly, **PEtMenG-PEG2000** and **PMenG-PEG750** assemblies, which were the least toxic in their non-irradiated form were markedly more toxic than the other assemblies after irradiation, with an IC_{50} value on the order of 50 μg/mL. Although L-menthol is generally considered safe and is widely used as a cooling agent in various products from cold medications to toothpaste, exposure to high doses can lead to toxic effects.[57,58] Indeed the IC_{50} value we obtained for the triggered polymers is in reasonable agreement with those determined in previous *in vitro* toxicity assays of menthol (50 – 120 μg/mL).[59] This toxicity was attributed to menthol's ability to cause the deterioration and induce leakage of mitochondrial membranes. Our assemblies therefore appear to be capable of depolymerizing and releasing biologically active menthol in response to stimuli. Given the interest in menthol as an analgesic, antifungal, antibacterial, and in other areas, the ability to release it in response to stimuli may prove useful for biomedical applications. Because of the complexities in the metabolic activity profiles of the different systems before and after irradiation, we chose to not evaluate the celecoxib-loaded particles in this assay.

Conclusion

In conclusion, we have successfully synthesized polyglyoxylates containing hydrophobic co-monomers including *n*-butyl glyoxylate, L-menthyl glyoxylate, and chloral. These polymers were end-capped with UV light-responsive linker, which allowed for their coupling with hydrophilic PEG to form amphiphilic block copolymers. The block copolymers were self-assembled into particles with diameters ranging from 82 – 173 nm in solution, and with cores having variable chemical structures and hydrophobicities, as indicated by measurements of their CAC values and the λ_{max} of encapsulated Nile red dye. All of the particles had similar triggerable disassembly capabilities based on DLS. The drug loading content for the hydrophobic drug celecoxib ranged from 6 wt% for **PEtGC-PEG2000** to 15 wt% for of **PEtBuG-PEG2000** and **PEtMenG-PEG2000**, suggesting that some cores were more compatible with celecoxib than others. All systems released celecoxib more rapidly when triggered with UV light as a stimulus than when not triggered, but differences in the precipitation of the drug and in drug retention were observed for the different systems. Finally, *in vitro* toxicity studies were performed on MDA-MB-231 cancer cells and it was found that the toxicity depended on the structure of the polymer and whether degradation had been triggered. Thus, it is possible to tune the self-assembly, drug loading, release, and toxicity of the polyglyoxylate assembly platform through simple tuning of the monomer polymer structures while retaining the essential stimuli-responsive properties. Future work will focus on the loading and release of different hydrophobic drugs, and on further *in vitro* and *in vivo* studies aimed at optimizing these systems for drug delivery applications.

Conflicts of interest

There are no conflicts to declare.

Acknowledgements

We thank the Natural Sciences and Engineering Research Council of Canada (Strategic Partnership Grant 478981-15, Discovery Grant 2016-04636, and fellowship to R. Y.) for funding this work.

References

1. G. Pitt, M. Gratzl, G. Kimmel, J. Surles and A. Sohindler, *Biomaterials*, 1981, **2**, 215-220.
2. A. R. Webb, J. Yang and G. A. Ameer, *Expert Opin. Biol. Ther.*, 2004, **4**, 801-812.
3. P. Gunatillake, R. Mayadunne and R. Adhikari, *Biotechnol. Annu. Rev.*, 2006, **12**, 301-347.
4. S. C. Hughes, P. M. Stott, A. J. Hearnden and L. G. Ripley, *Injury*, 2007, **38**, 212-222.
5. J. Nicolas, S. Mura, D. Brambilla, N. Mackiewicz and P. Couvreur, *Chem. Soc. Rev.*, 2013, **42**, 1147-1235.
6. A. Varela-Moreira, Y. Shi, M. H. Fens, T. Lammers, W. E. Hennink and R. M. Schiffelers, *Mater. Chem. Front.*, 2017, **1**, 1485-1501.
7. R. A. Petros and J. M. DeSimone, *Nat. Rev. Drug Discovery*, 2010, **9**, 615.
8. H. Cabral and K. Kataoka, *J. Controlled Release*, 2014, **190**, 465-476.
9. M. Hakkarainen, A. Höglund, K. Odelius and A.-C. Albertsson, *J. Am. Chem. Soc.* , 2007, **129**, 6308-6312.
10. M. Källrot, U. Edlund and A.-C. Albertsson, *Biomacromolecules*, 2007, **8**, 2492-2496.
11. E. Cabane, X. Zhang, K. Langowska, C. G. Palivan and W. Meier, *Biointerphases*, 2012, DOI:10.1007/s13758-011-0009-3.
12. S. Mura, J. Nicolas and P. Couvreur, *Nat. Mater.*, 2013, **12**, 991-1003.
13. K. M. Huh, H. C. Kang, Y. J. Lee and Y. H. Bae, *Macromol. Res.*, 2012, **20**, 224-233.
14. J. Liu, Y. Huang, A. Kumar, A. Tan, S. Jin, A. Mozhi and X. J. Liang, *Biotechnol. Adv.*, 2014, **32**, 693-710.
15. W. Agut, A. Brûlet, C. Schatz, D. Taton and S. Lecommandoux, *Langmuir*, 2010, **26**, 10546-10554.
16. C. de Gracia Lux, S. Joshi-Barr, T. Nguyen, E. Mahmoud, E. Schopf, N. Fomina and A. Almutairi, *J. Am. Chem. Soc.*, 2012, **134**, 15758-15764.

17. Y. Lee, H. Mo, H. Koo, J.-Y. Park, M. Y. Cho, G.-w. Jin and J.-S. Park, *Bioconjugate Chem.*, 2007, **18**, 13-18.
18. J. Olejniczak, V. A. N. Huu, J. Lux, M. Grossman, S. He and A. Almutairi, *Chem. Commun.*, 2015, **51**, 16980-16983.
19. B. Fan and E. R. Gillies, *Encycl. Polym. Sci. Technol.*, 2015, 1-35.
20. M. E. Roth, O. Green, S. Gnaim and D. Shabat, *Chem. Rev.*, 2015, **116**, 1309-1352.
21. S. T. Phillips and A. M. DiLauro, *ACS Macro Lett.*, 2014, **3**, 298-304.
22. A. Sagi, R. Weinstain, N. Karton and D. Shabat, *J. Am. Chem. Soc.*, 2008, **130**, 5434-5435.
23. A. M. DiLauro, A. Abbaspourrad, D. A. Weitz and S. T. Phillips, *Macromolecules*, 2013, **46**, 3309-3313.
24. A. P. Esser-Kahn, N. R. Sottos, S. R. White and J. S. Moore, *J. Am. Chem. Soc.*, 2010, **132**, 10266-10268.
25. S. Tang, M. Yourdkhani, C. M. Possanza Casey, N. R. Sottos, S. R. White and J. S. Moore, *ACS Appl. Mater. Interfaces*, 2017, **9**, 20115-20123.
26. G. G. Lewis, J. S. Robbins and S. T. Phillips, *Chem. Commun.*, 2014, **50**, 5352-5354.
27. G. Liu, X. Wang, J. Hu, G. Zhang and S. Liu, *J. Am. Chem. Soc.*, 2014, **136**, 7492-7497.
28. B. Fan and E. R. Gillies, *Mol. Pharmaceutics*, 2017, **14**, 2548-2559
29. B. Fan, J. F. Trant and E. R. Gillies, *Macromolecules*, 2016, **49**, 9309-9319.
30. S. Gnaim and D. Shabat, *J. Am. Chem. Soc.*, 2017, **139**, 10002-10008.
31. E. K. Chen, R. A. McBride and E. R. Gillies, *Macromolecules*, 2012, **45**, 7364-7374.
32. M. S. Baker, H. Kim, M. G. Olah, G. G. Lewis and S. T. Phillips, *Green Chem.*, 2015, **17**, 4541-4545.
33. C. Ergene and E. F. Palermo, *Biomacromolecules*, 2017, **18**, 3400-3409.
34. B. Fan, J. F. Trant, A. D. Wong and E. R. Gillies, *J. Am. Chem. Soc.*, 2014, **136**, 10116-10123.
35. A. M. DiLauro and S. T. Phillips, *Polym. Chem.*, 2015, **6**, 3252-3258.
36. C. de Gracia Lux, C. L. McFearin, S. Joshi-Barr, J. Sankaranarayanan, N. Fomina and A. Almutairi, *ACS Macro Lett.*, 2012, **1**, 922-926.
37. B. Fan, J. F. Trant, R. E. Yardley, A. J. Pickering, F. Lagugné-Labarthet and E. R. Gillies, *Macromolecules*, 2016, **49**, 7196-7203.
38. M. A. DeWit, A. Beaton and E. R. Gillies, *J. Polym. Sci., Part A: Polym. Chem.*, 2010, **48**, 3977-3985.
39. H. Zhang, K. Yeung, J. S. Robbins, R. A. Pavlick, M. Wu, R. Liu, A. Sen and S. T. Phillips, *Angew. Chem. Int. Ed.*, 2012, **51**, 2400-2404.
40. B. Fan, J. F. Trant, G. Hemery, O. Sandre and E. R. Gillies, *Chem. Commun.*, 2017, **53**, 12068-12071.
41. G. I. Peterson, D. C. Church, N. A. Yakelis and A. J. Boydston, *Polymer*, 2014, **55**, 5980-5985.
42. P. K. Nguyen, C. G. Snyder, J. D. Shields, A. W. Smith and D. L. Elbert, *Macromol. Chem. Phys.*, 2013, **214**, 948-956.
43. J. Fenneteau, S. Vallerotto, L. Ferrié and B. Figadère, *Tetrahedron Lett.*, 2015, **56**, 3758-3761.
44. H. Oertling, A. Reckziegel, H. Surburg and H.-J. Bertram, *Chem. Rev.*, 2007, **107**, 2136-2164.
45. I. Rosen, D. Hudgin, C. Sturm, G. McCain and R. Wilhjelm, *J. Polym. Sci., Part A: Polym. Chem.*, 1965, **3**, 1535-1543.
46. H.-G. Elias, *Macromolecules*, Springer Science & Business Media, 2012.
47. S. Zalipsky, *Bioconjugate Chem.*, 1995, **6**, 150-165.
48. V. Jendrossek, in *Mitochondria: The anti-cancer target for the thrid millenium*, eds. J. Neuzil, S. Pervaiz and S. Fulda, Springer, Dordrecht, 2014, ch. 5, pp. 105-133.
49. V. Bhatt, G. Shete and A. K. Bansal, *Int. J. Pharm.*, 2015, **495**, 132-139.
50. S.-W. Zhang, A. P. Brunskill, E. Schwartz and S. Sun, *Cryst. Growth Des.*, 2017, **17**, 2836-2843.
51. P. R. Baker, S. D. Cramer, M. Kennedy, D. G. Assimos and R. P. Holmes, *Am. J. Physiol.: Cell Physiol.*, 2004, **287**, C1359-C1365.
52. R. J. Wanders and H. R. Waterham, *Annu. Rev. Biochem.*, 2006, **75**, 295-332.
53. B. Belloncle, C. Bunel, L. Menu-Bouaouiche, O. Lesouhaitier and F. Burel, *J. Polym. Environ.*, 2012, **20**, 726-731.
54. H. Greim, *The MAK-Collection for Occupational Health and Safety*, Wiley-VCH, 2012.
55. S. Wilson, J. Easton, K. Lamb, R. Orchardson and P. Casamassimo, *Pediatric Dentistry*, 2000, **22**, 107-112.
56. R. Abbas and J. W. Fisher, *Toxicol. Appl. Pharmacol.*, 1997, **147**, 15-30.
57. A. Kumar, U. Baitha, P. Aggarwal and N. Jamshed, *Int. J. Appl. Basic Med. Res.*, 2016, **6**, 137.
58. G. P. Kamatou, I. Vermaak, A. M. Viljoen and B. M. Lawrence, *Phytochemistry*, 2013, **96**, 15-25.
59. V. S. Bernson and B. Pettersson, *Chem.-Biol. Interact.*, 1983, **46**, 233-246.